

2006

Investigation of Suction Process of Scroll Compressors

Michael M. Cui

Trane

Jack Sauls

Trane

Follow this and additional works at: <http://docs.lib.purdue.edu/icec>

Cui, Michael M. and Sauls, Jack, "Investigation of Suction Process of Scroll Compressors" (2006). *International Compressor Engineering Conference*. Paper 1746.

<http://docs.lib.purdue.edu/icec/1746>

This document has been made available through Purdue e-Pubs, a service of the Purdue University Libraries. Please contact epubs@purdue.edu for additional information.

Complete proceedings may be acquired in print and on CD-ROM directly from the Ray W. Herrick Laboratories at <https://engineering.purdue.edu/Herrick/Events/orderlit.html>

Investigation of suction process of scroll compressors

Michael CUI¹, Jack SAULS²

TRANE
La Crosse, WI 54650 USA

¹(608) 787-3313
mcui@trane.com

²(608) 787-2517
jsauls@trane.com

ABSTRACT

The suction process of a scroll compressor was investigated. The investigation started from the numerical simulation of the entire scroll compressor working process. The simulation included the upper main bearing housing, thrust plate, scrolls, dummy and discharge ports, check valve, and plenum. The basic geometric features and physical mechanisms that the scroll compressor performance is associated with were simulated first. The working fluid was Refrigerant 134a. The suction process was studied as a part of the integrated working environment. The fundamental mechanism of the suction process was defined. The interaction of the compressor design features was quantified. The overall parameters were calculated from the field quantities. The methodology developed and the data obtained can be applied to the design and optimization of scroll compressors.

1. INTRODUCTION

In a scroll compressor, the gas stays in a series of crescent-shaped volumes. The working process consists of suction, compression, and discharge stages. As the first stage of the working process, the suction not only may cause loss in its own process but also sets the start conditions of the compression process. Therefore, the suction process is an important part for scroll compressor performance.

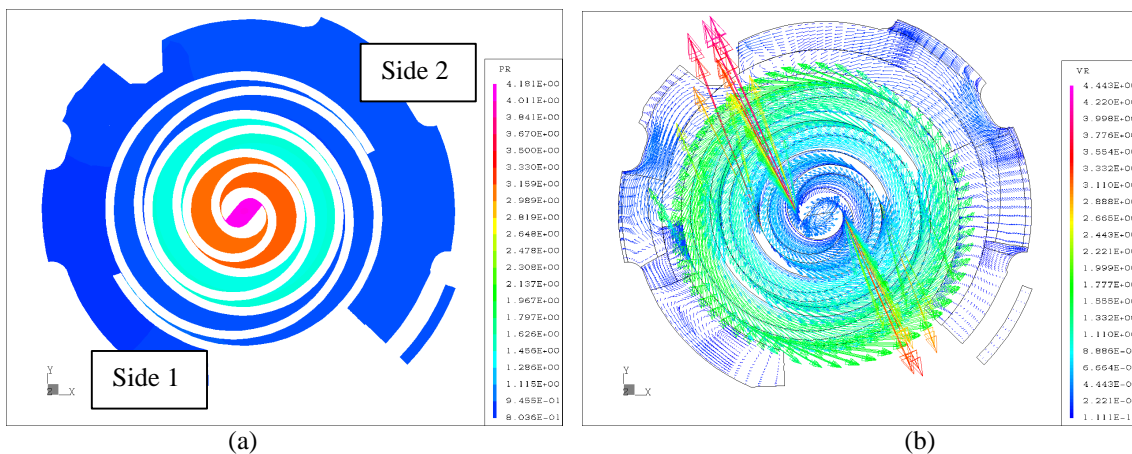


Figure 1. Pressure (a) and velocity (b) distributions inside the scroll compressor.

Yanagisawa et al. (1990) calculated the suction volume of a scroll compressor using geometric parameters of the fixed and orbiting scrolls. Halm (1997) added additional terms in the equation and obtained the approximate expressions for both the inlet area and volume of the suction chamber. Chen et al. (2002a)

calculated the suction gas flow using the flow equation for isentropic flow of a compressible ideal gas, corrected by a flow factor as described by Fox and McDonald (1992). Chen's analysis also integrated the suction process with the compression and discharge processes of a scroll compressor and obtained a quasi-static model for the scroll compressor working process (2002b). Cui (2003) developed a complete numerical model for a scroll compressor using Refrigerant 22 as the working fluid. The suction process was a part of the analysis.

In the current investigation, the dynamic flow field during the suction process was numerically simulated. The geometric details and their motions were included without approximations. The general features of the geometry, the pressure and velocity distributions are shown in Figure 1. Since the gas enters the compressor from two sides, the subscripts of 1 and 2 are introduced to label corresponding features on both sides. The numerical model has a total of 2.5 million nodes. The methodology has been described by Cui (2003). The Martin-Hou equation of state was used for R134a gas. The transport properties were calculated with power laws. The physics of the gas intake was studied in an integrated environment with the upstream and downstream components. The performance parameters were then calculated from the field quantities. The potential to optimize design of the suction process is discussed.

The data were recorded as a time series. For each time step, the basic field quantities were recorded as functions of time and location. The other field quantities can be calculated from these basic field quantities. The spatially averaged quantities were obtained for each file of the time series. The statistic quantities can be obtained following the proper averaging procedures. The design and performance parameters associated with the suction process were obtained by integrating the field quantities over the domain of interest. The detailed algorithms have been described by Cui (2003).

2. GEOMETRIC FEATURES OF THE SUCTION PROCESS

The suction chambers open at the beginning of the suction process. They are located at the outmost edge of the scrolls and are formed by the sections near the end of the orbiting and fixed scrolls. The opening area increases gradually to its maximum value. After the peak value is reached, the area starts to decrease and is eventually closed. At this point, the suction stage ends and the compression stage starts. The crankshaft rotates 360 degrees. The total process shows a bell-curve profile (Figure 2(a)). The variation of the suction chamber volume looks like an inverse hyperbolic cosine function (Figure 2(b)). The total volume increases continuously until it reaches its maximum value at 340 degrees of the crank angle. After it reaches its maximum value, the volume starts to decrease until the opening is closed. Since the suction chamber starts from a small volume and increases its size gradually, the intake loss is smaller than in the processes that open the chamber suddenly. However, the opening area and volume of the chamber are not linear functions of the crank angle. The opening area increases fast at the first half of the intake process and decreases rapidly in the second half of the process. This pulsation-like profile requires the suction flow path to supply adequate gas rapidly with a tolerable level of loss. The different profiles of the opening area and the volume of the suction chambers also needs to be taken into consideration to ensure an efficient suction process. During the last part of the suction process, the volume actually decreases. The gas is driven out of the suction chamber. The energy used to drive this part of the gas in and out of the suction chamber is wasted. A good suction process design should minimize the volume of gas squeezed out.

The flow path around the scrolls is irregular (Figure 1). The shape of the flow path is determined by many different design considerations. These considerations are not always aerodynamic. Although the scrolls are symmetric on both sides of the compressor, the total flow path for the refrigerant gas is not the same on the two sides. Along the vertical direction, a similar situation exists. The pictures would be more complicated if the upstream components included the motor barrel, oil sump, shell, and other smaller components. In the current study, only the upper bearing housing and thrust plate are included as upstream components. The geometry included in the current research is shown in Figure 3. The color code indicates the radial distance from the center of the compressor. The flow in the space around the scroll is three-dimensional and time dependent.

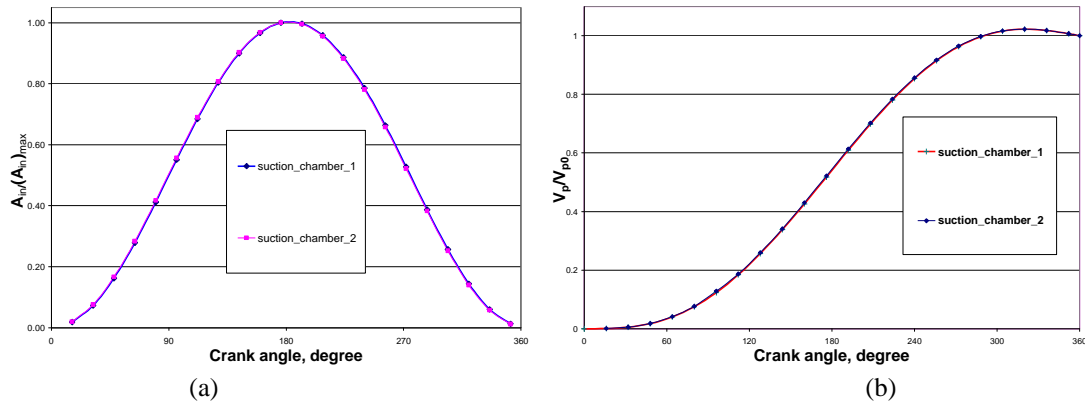


Figure 2. Opening area (a) and volume (b) of the suction chamber inside the scroll compressor.

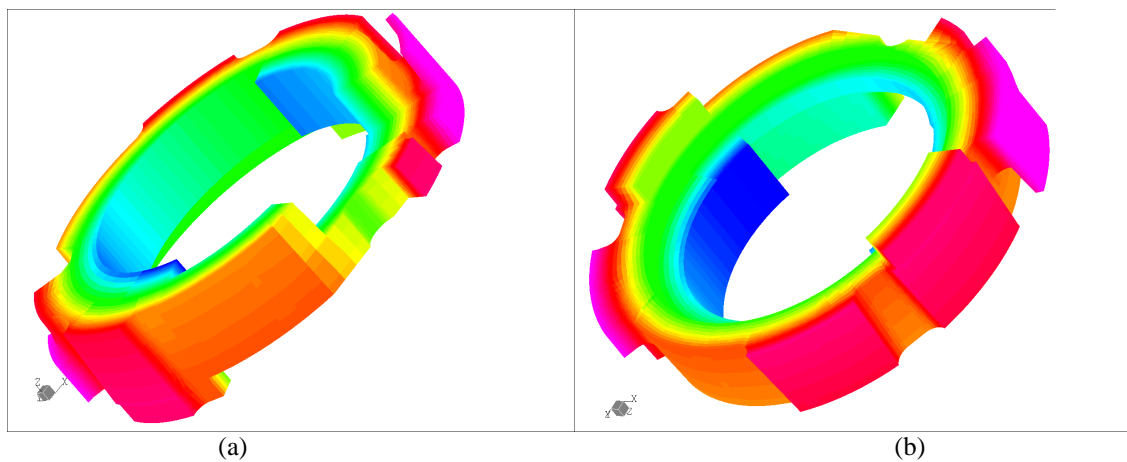


Figure 3. Geometry of suction side of the scroll compressor: (a) view from top and (b) view from bottom.

3. FLOW PHYSICS OF THE SUCTION PROCESS

After the suction chamber opens, the suction chamber volume starts to increase. A region of low-pressure forms inside the suction chamber generating a pressure differential between the space around the scrolls and inside the suction chamber. The refrigerant gas starts to flow into the suction chamber. The flow field is three-dimensional and time-dependent. The variation of the flow field is determined by the surrounding structure and physical conditions. The main features of the pressure field can be observed in Figure 4.

The pressure at the inlet of the suction chamber has the highest value in the chamber. This phenomenon holds for the entire suction process. This high-pressure region is generated by the gas flow outside of the suction chamber where the flow is slow and pressure is high.

The high pressure at the inlet drives the flow into the suction chamber. This high-speed gas flow accelerates into the chamber and generates two separation regions near the entrance. The first separation region is located at the inside wall of the fixed scroll. The motion of the orbiting scroll pulls the gas flow towards the orbiting scroll walls that moves away from the fixed scroll. The second location of the separation is at the inside wall of the orbiting scroll downstream from the location of the first separation. The second separation is formed when the inlet flow hits the moving wall of the orbiting scroll and turns around to flow back into the suction chamber.

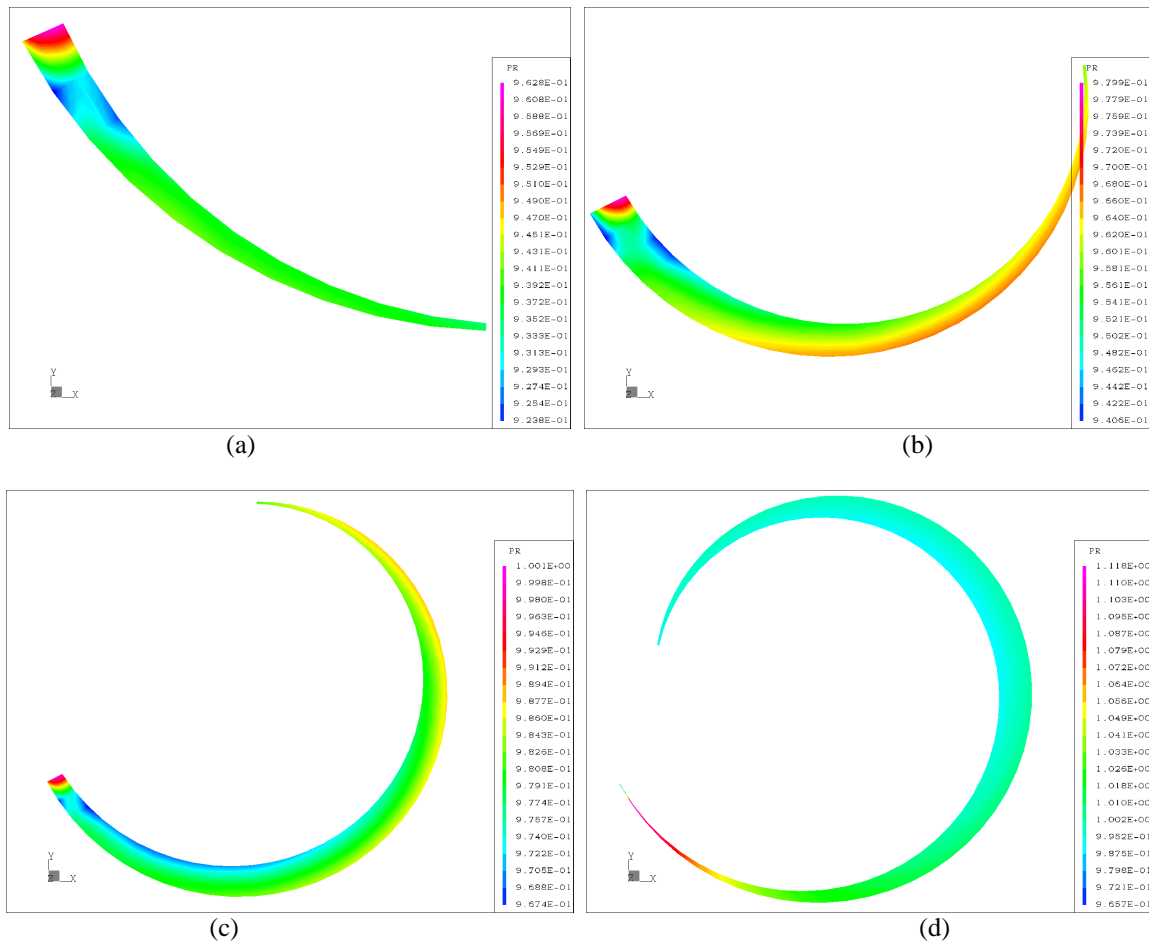


Figure 4. Pressure distribution inside the suction chamber at the crank angles of: (a) 96°, (b) 192°, (c) 272°, (d) 352°.

The low-pressure region is formed along the inside wall of the orbiting scroll during the suction process. The volume increase of the suction chamber is the result of the motion of the orbiting scroll. The inside surface of the orbiting scroll moves away from the fixed scroll. This motion creates the low-pressure region on the surface of the moving orbiting scroll.

The velocity distributions inside the suction chamber are shown in the crank angles of 96°, 192°, 272°, and 352° (Figure 5).

The separation regions can be observed in the velocity plots. The inlet velocity turns towards inside wall of the orbiting scroll. The second separation region located on the orbiting scroll also can be observed in the plots.

The velocity profiles inside the suction chamber show a predominantly parabolic shape. The velocity has its highest value near the centerline of the suction chamber. This phenomenon indicates that the flow is driven by the pressure differential. The moving boundary of the orbiting scroll induces comparatively weaker velocity variation, although this variation is observable inside the suction chamber.

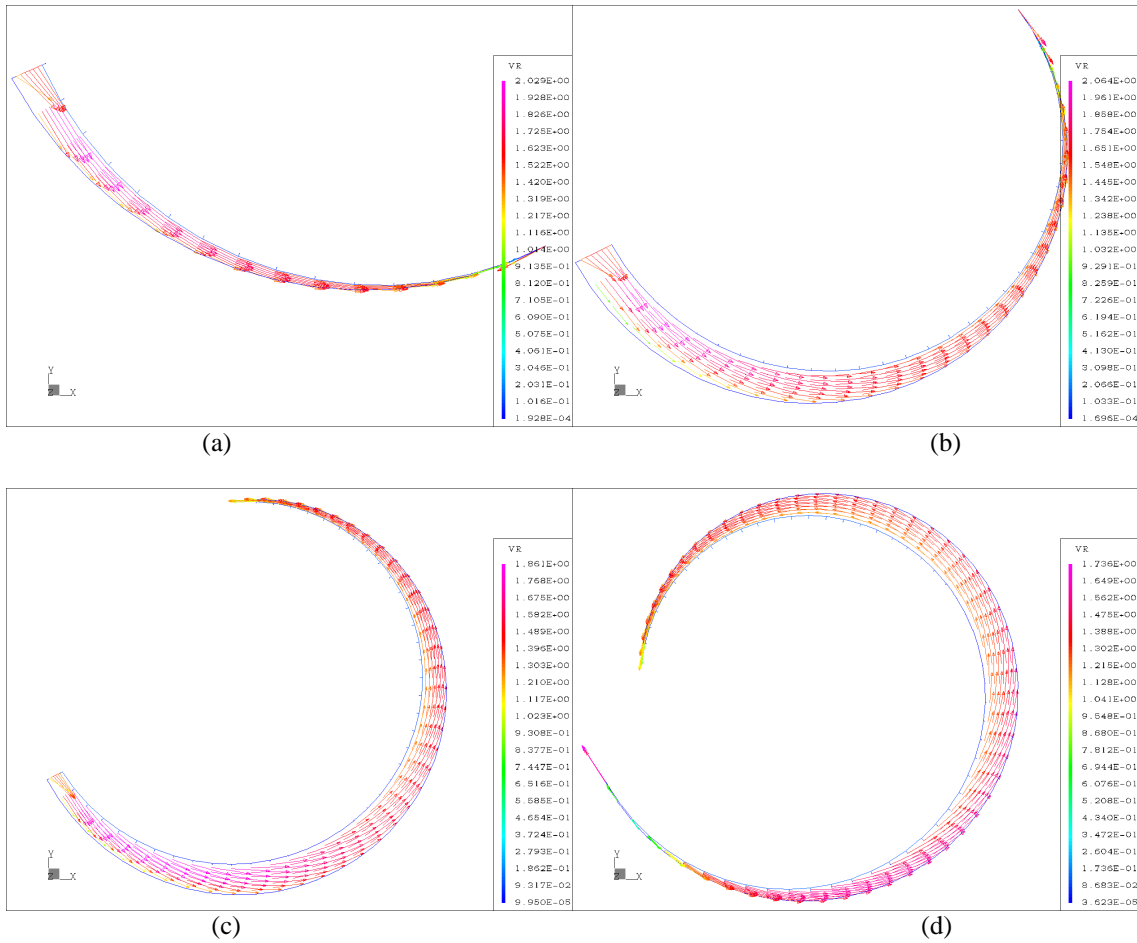


Figure 5. Velocity distribution inside the suction chamber at the crank angles of: (a) 96°, (b) 192°, (c) 272°, and (d) 352°.

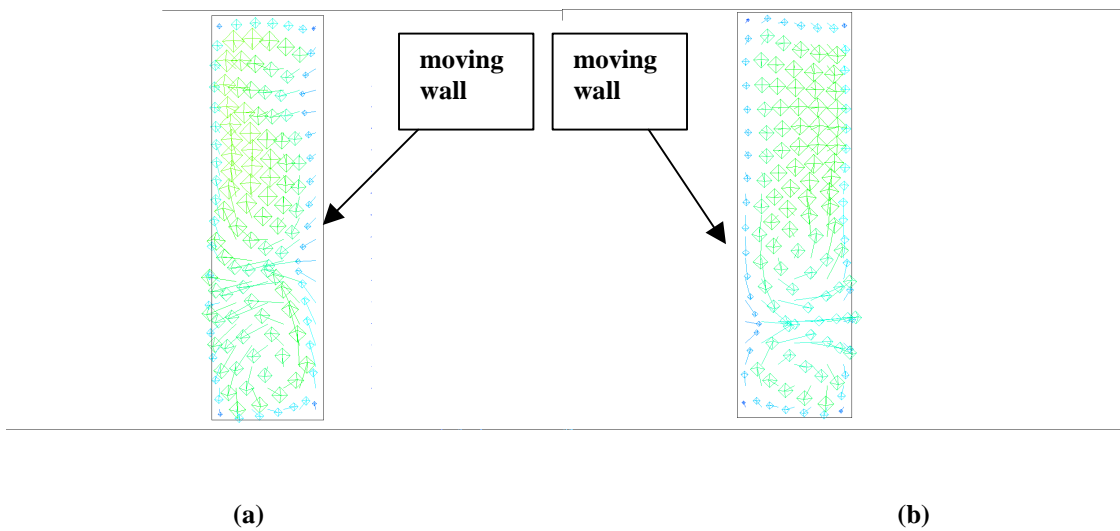


Figure 6. Vortices in suction chamber 1(a) and suction chamber 2(b) of the scroll compressor.

A very interesting phenomenon observed in the velocity field is the vortices formed inside the suction chamber. Figure 6 shows the cross section areas of both suction chambers. The two vortices, one rotates clockwise and the other rotates counter-clockwise, can be seen in each cross-section. The first vortex is located on the upper part the first suction chamber. It takes up about two-thirds of the cross-section area. The second vortex is located on the lower part of the cross-section area. It takes up about one-third of the area. However, the smaller vortex is stronger than the larger one. These vortices dissipate energy provided by the motor into heat. One of the design objectives should be to reduce or eliminate these vortices.

4. AVERAGED PARAMETERS

The area- and volume-averaged pressure and temperature are calculated. Since the assessment of design is based on the averaged properties, these parameters are often used to quantify the design of the compressors.

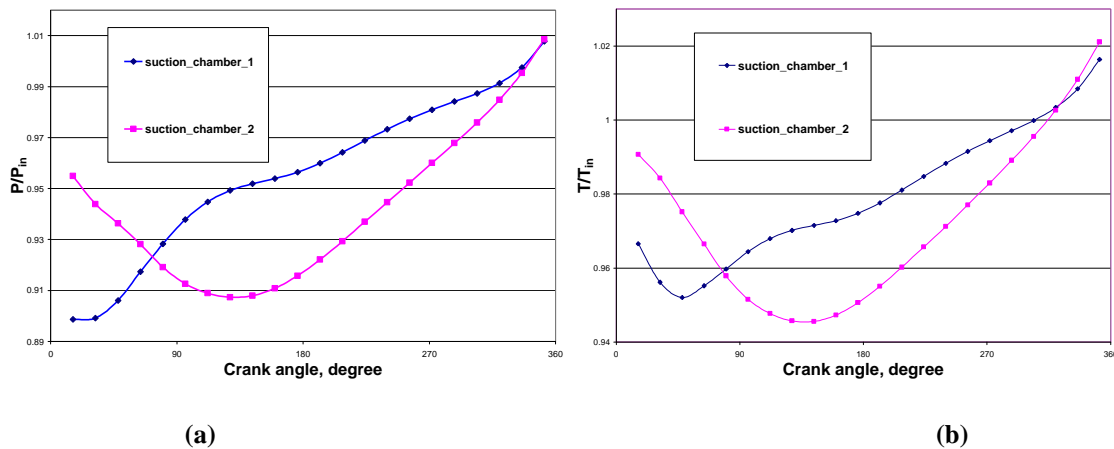


Figure 7. Pressure (a) and temperature (b) inside the suction chambers.

The volume-averaged pressure values inside the suction chamber are shown in Figure 7(a). To generalize the results, the pressure is non-dimensionalized using the inlet pressure of the compressor. The pressure inside two sides of the compressor shows different profiles as the function of the crank angle. However, the pressure values at the end of the suction process are the same. Since the volumes of both suction chambers grow during the suction process, the refrigerant gas does work on the compressor. The suction chambers work like expanders during the suction process. The suction chamber 1 does more work on the compressor than the suction chamber 2.

The temperature variation during the suction process is shown in Figure 7(b). The value of the temperature is nondimensionalized by the averaged compressor inlet temperature. The overall profiles are similar to pressure distribution. The temperature value is also volume-averaged over the suction chamber at each time step. The data in Figure 7 are only a fraction of the total temperature history. However, these data are dense enough to illustrate the physical nature of the suction process.

Although the asymmetric features exist in both pressure and temperature distributions, the time histories of these physical quantities demonstrate the overall temporal characteristics of the suction process. At the beginning of the suction process, the gap widens and the volume increases rapidly. The refrigerant gas is drawn into the suction chamber with acceleration. The velocity of the gas increases rapidly. The pressure and temperature inside the suction chamber decrease. The gas actually expands inside the suction chamber. As the gas gains its momentum flowing into the suction chamber, the opening rate of the gap slows down and eventually starts to decrease. The levels of the temperature and pressure inside the suction chamber start to grow. The mass flow rate through the opening passes its peak value at a crank angle close to 180 degrees. As the crankshaft continues to rotate, the mass flow rate starts to decrease. The growing rate of the total mass inside the chamber slows down and eventually reaches its maximum value. When the accumulated mass inside the suction volume is at its peak value, the pressure and temperature surpass the

compressor inlet pressure and temperature values. The gas is actually pre-compressed before the compression stage starts. Consequently, the gas is driven out of the section chamber and the value of the total mass inside the suction chamber is smaller than its maximum value (Figure 8).

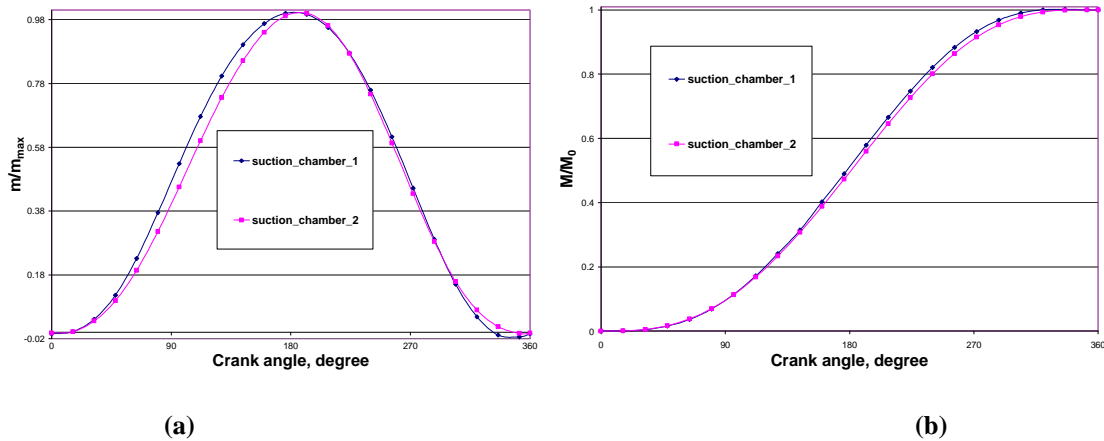


Figure 8. Mass flow at inlet (a) and accumulated mass (b) inside the suction chambers.

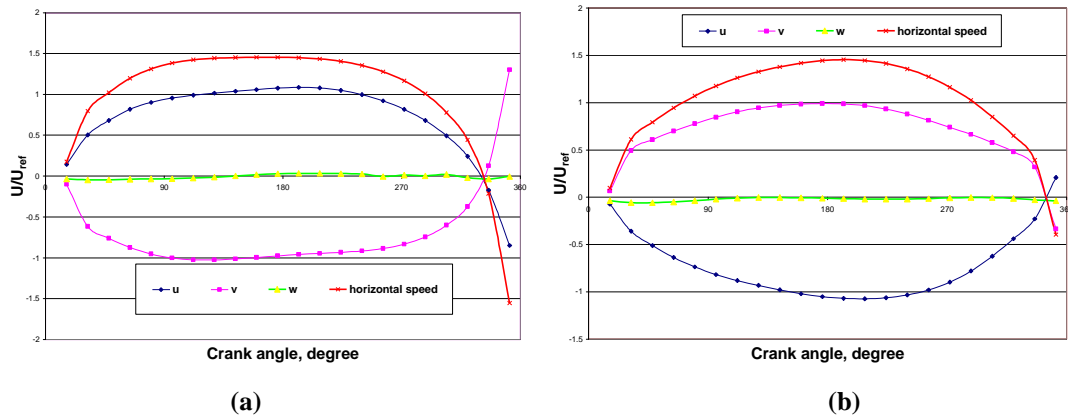


Figure 9. Velocity distributions in suction chamber 1 (a) and suction chamber 2 (b).

The velocity distributions inside both suction chambers are shown in Figure 9. The velocity has three components, u , v , and w . The u - and v -components are on the horizontal plane and z -component aligns with vertical direction. Since the inlet surfaces of the suction chambers are perpendicular to the horizontal plane, the mass flow rate into the suction chamber is only determined by the u - and v -components. The w -component does not help the suction process. The negative values in the velocity plots show the gas is driven out of the chamber before it is closed. This phenomenon causes additional loss of performance in the suction process.

The asymmetric profiles on the two sides of the compressor are seen in all of the averaged field properties. The differences of the two sides are caused by both the geometric features of the surrounding structures (bearing housing, motor barrel, and other components) and the physical parameters. Before the gas reaches the entrance of the suction chamber, the distortions caused by the upstream components affect the inlet conditions of the suction chambers. The motion of the orbiting scroll also interacts with the physical structures around the suction chambers. The two suction chambers operate at the different conditions even though they are geometrically similar.

5. CONCLUDING REMARKS

The refrigerant gas is drawn into the suction chamber by pressure difference. The pressure distribution along the circumference of the compressor is the result of the growing volume of the suction chamber. This change is caused by the volume gain as the orbiting scroll moves around a circular track. The variation of the pressure along the radial direction is induced by the radial velocity component of the orbiting scroll wall. The dynamic features of the process show expansion at the beginning and compression at later stage of the suction process. The suction chambers work like expanders and do work on the compressor.

There are separations and vortices in the flow field during the gas intake process. The objective of the suction process design should include the reduction of these phenomena to improve the efficiency of the compressor.

The field properties on the two sides of the compressor are not the same. The suction chambers on the opposite side of the compressor are operating at different inlet conditions. Although it is difficult to design all upstream components symmetrically, the effort to achieve the better inlet conditions should be made.

ACKNOWLEDGEMENTS

The authors would like to thank TRANE Air Conditioning, American Standard Companies, for the permission to publish this paper.

REFERENCES

- [1] Yagagisawa, et al. "Optimum operating pressure ratio for scroll compressors," *Proceedings of the International Compressor Engineering Conference at Purdue*, 1990.
- [2] Halm, N. P., "Mathematical modeling of scroll compressors," Master thesis of Herrick Lab, Purdue University, 1997.
- [3] Chen, Y., Halm, N. P., Groll, E. A., Braun, J.E., "Mathematical modeling of scroll compressors Part I: compression process modeling," *Journal of Refrigeration*, 25 (2002) 731-750.
- [4] Chen, Y., Halm, N. P., Groll, E. A., Braun, J.E., "Mathematical modeling of scroll compressors Part II: overall compressor modeling," *Journal of Refrigeration*, 25 (2002) 751-764.
- [5] Fox., R.W., McDonald, A.T., "Introduction to Fluid Mechanics," New York, John Wiley & Sons, 1992.
- [6] Cui, M.M., "Numerical study of unsteady flows in a scroll compressor," *Proceedings of the International Conference on Compressors and their systems, London*, 2003, pp2-10.

NOMENCLATURE

A	opening area
\dot{m}	mass flow rate
M	mass
P	pressure
T	temperature
t	time
U	velocity

u, v, w component of the velocity
V suction chamber volume

Subscripts

a averaged quantity
in value at compressor inlet
max maximum value
0 compression stage starting value
r ratio
ref reference value
t turbulence

Superscripts

- average